The complete reflectance vs. wavelength curves are shown in Fig. 5 for both the field-off state (0V) and the field-on state (2.6V). From Fig. 5, we find at the field-off state, the reflectance vs. wavelength of both curves are identical. But at the field-on state, the reflectance of the RTN cell is 10% greater than that of the 45° cell.
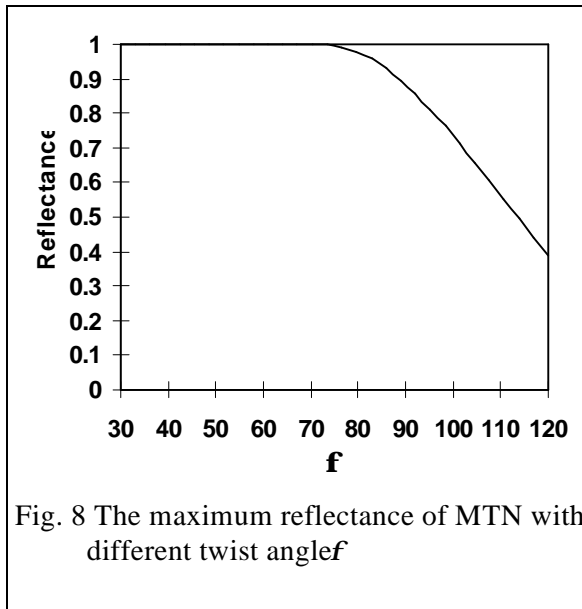

Fig. 8 The maximum reflectance of MTN with different twist angle f

To verify our theoretical simulation, two groups of sample cells were fabricated, one with 52° twist and the other with 45° twist. Their measured RVCs for 514nm wavelength are shown in Fig. 6. Also their reflectance vs. wavelength curves are shown in Fig. 7. The agreement between theory and experiment is good. The slight deviation in the threshold voltage is because of the refractive index uncertainty.

OPTIMIZED MTN MODE

The MTN mode is normally black as shown in Fig. 3. There are also 3 parameters $(f, a, d\Delta n)$ for the MTN cell. For a given twist angle f, we used a 2-D search within a proper range of $(a, d\Delta n)$ for finding the best operating points of the MTN display. Fig. 8 shows the 1st order maximum reflectance of the MTN display as a function of the twist angles f. From Fig. 8, it can be seen that the efficiency of the MTN mode decreases gradually when the twist angle is larger than 70°. Moreover, it is found that for low twist angles, the $d\Delta n$ required becomes quite small. This will lead inevitably to difficult cell fabrication as well as a poor dark state. So we shall concentrate on the range of $f = 60°$ ~ 90° for optimizing the MTN mode. For the ideal case of no light loss, $f = 90°$ yields a reflectance of 89%, while for the $f = 80°$ MTN cell, 97% reflectance is obtained.

Fig. 9 shows the $\alpha - d\Delta n$ parameter space for the MTN mode. The contour lines of constant reflectance are in steps of 0.1. The values of ϕ are 60°, 70°, 80°, and 90° respectively. A, B, C and D are the possible static operating points of the 60°, 70°, 80°, and 90° MTN cells. Through the further refinement, we select some best operating points for different twist angles. Their $(f, a, \Delta nd)$ values are $(60°, -5°, 0.19)$, $(70°, 7°, 0.22)$, $(80°, 15°, 0.24)$ and $(90°, 20°, 0.25)$. The optimization wavelength is 550nm. The Δn values are given in μm.

Fig.10 shows the reflectance vs. wavelength characteristic of these cells. From Fig.10 we find that at the voltage-off state the RVCs for the cells of 60°, 70°, 80°, are about 10% higher than that of the 90° cell. Moreover, it can be seen that in all cases, the dark states are very nondispersive, which is a major characteristic and advantage of the MTN mode[9].

We plot the RVCs of the $(80°, 15°, 0.24)$ MTN cell in Fig. 11. R, G and B represent red, green and blue lights at 650nm, 550nm and 450nm respectively. Compared with the RVCs of the 90° MTN cell, we find that the reflectance of 80° MTN in Fig.11 is higher while the dispersion is similar. Thus, the light efficiency of the 80° MTN cell (40% for G light) is higher than that of the 90° MTN cell (35% for G light). The RVCs of the 60° and 70° MTN cells have also been simulated. Their reflectance is also higher than that of 90° MTN cell, but their voltage-on states are not very dark and also their $d\Delta n$ values are too small to fabricate. After considering these constrains, we believe that $(80°, 15°, 0.24)$ represents the optimal MTN cell.
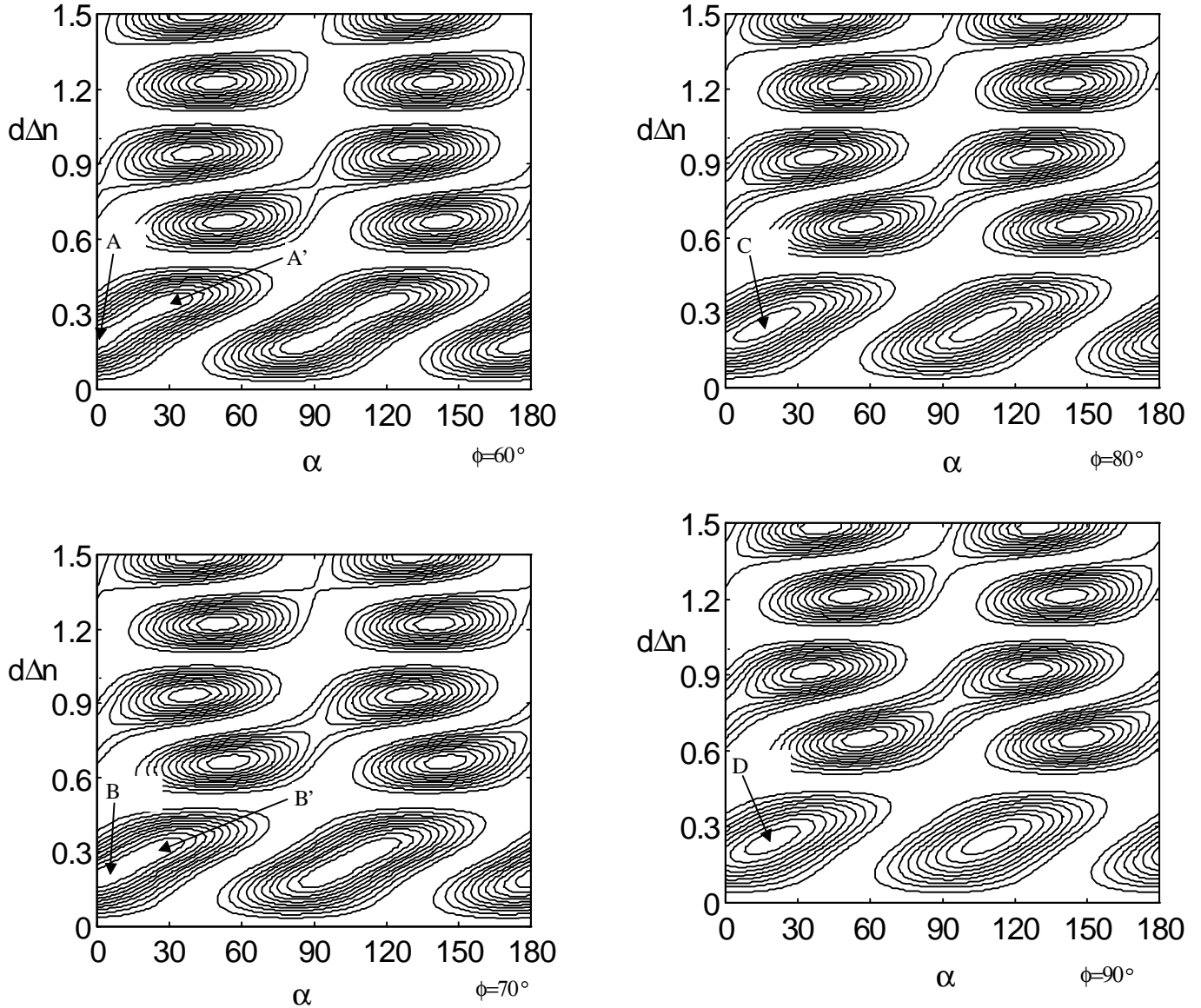
Fig. 9 α−dΔn parameter space for RLCDs. The contour lines of constant reflectance are in steps of 0.1. The values of φ are fixed at 60°, 70°, 80°, and 90° respectively.

To verify the theoretical simulation, sample cells for the optimal 80° and the 90° MTN cells were made. We used a mixture of MLC 5300 and MLC 5400 to get the exact Δn. The cell gap was controlled by 2.2μm spacers. Fig.12 shows the spectral responses of these sample cells. In Fig.13, the RVCs for white light are also given. From Fig.12 and Fig.13, we found that the optimal 80° MTN cell has 10% higher light efficiency than that of 90° MTN cells.

For the MTN mode, the largest $d\Delta n$ is about 0.24μm for the 90° MTN cell. The smallest $d\Delta n$ is about 0.18μm for the 60° MTN cell. When the cell twist angle becomes smaller, the operating voltage becomes higher and higher. For the 60°, 70°, 80° and 90° MTN cells, through numerical simulations, we found that when the
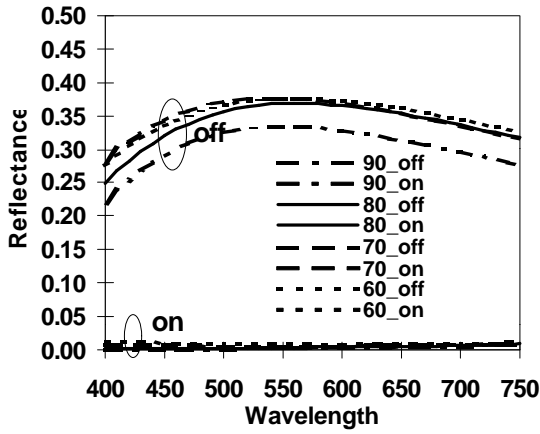
Fig.10 Reflectance vs. wavelength relation at the voltage-off and voltage-on states
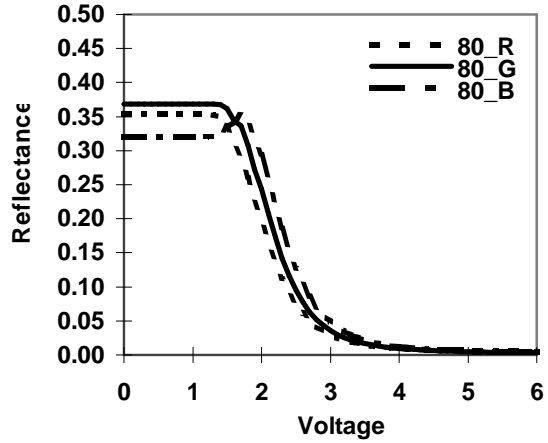

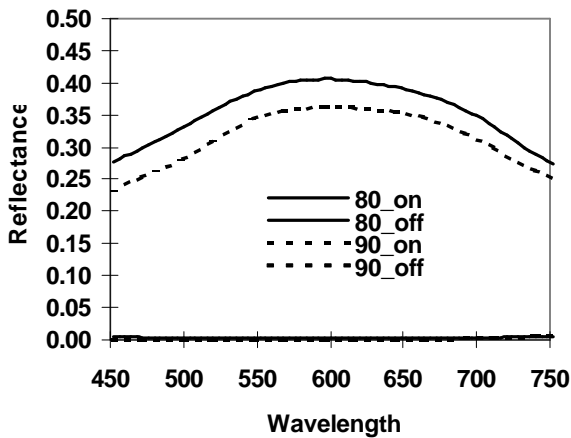Fig. 11 Reflectance vs. voltage relation of (80°,15°,0.24) cell

Fig.12 The experimental RVCs of optimal and 90° MTN cells at voltage-on and off states.
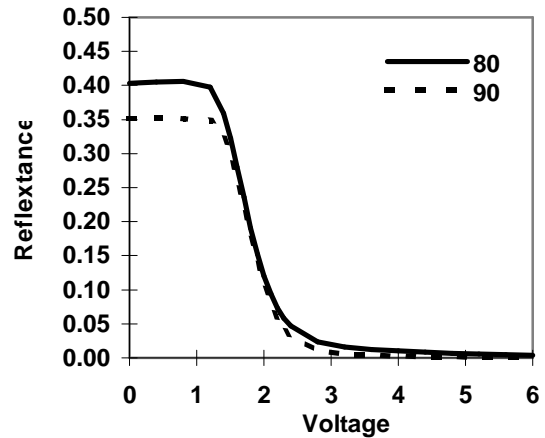

Fig.13. The experimental RVCs of the optimal and 90° MTN cells for white light

dark state operating voltage is 4V, their white light contrast ratio will be 15, 21, 32 and 65 respectively. If we increase the operating voltage to 6 V, their white light contrast ratio will be 37, 53, 78 and 116 respectively. Such thin cell gap (normally about 2-3μm) cannot usually operate at such voltages due to cell shorting. Special techniques

Voltage Cell parameters	4V	5V	6V
70°,0.28,22°	36	68	74
70°,0.31,30°	74	96	106
70° **MTN**	20	37	52
90° **MTN**	65	103	115
60° **SCTN**	76	100	111

Table 1 Contrast ratios of different cells under operating voltages of 4V, 5 V, and 6 V.

have to be adopted to eliminate the electrical shorting problem. The thin cell gap also makes the cell difficult to manufacture. The high dark state operating voltage also makes the cost of the LCD driver higher. Thus, new RLCD with thicker cell gaps and lower operating voltages should be developed.

Recently, Yang proposed a new SCTN mode [10]. In this SCTN mode, the dark state can be obtained at a low operating voltage. However, the color dispersion for this SCTN cell is quite serious. Actually, the SCTN mode is the same as the MTN mode except that a different TN-ECB maximum is used as the static operating point as indicated in Fig. 3. Fig. 9 shows the static working point (point A′) of the SCTN mode. As seen in Fig. 9, the positive and negative TN-ECB modes (A′ and A) merge into one region. Any point in this A-A′ region and likewise the B-B′ region can serve as the static operating point for the SCTN mode. The RVCs of the cells with the parameters (70°, 30°, 0.31) and (60°, 30°, 0.33) are plotted in Fig. 14 and Fig. 15 respectively. Fig. 15 actually corresponds to the SCTN mode of Yang, while Fig. 14 corresponds to a new "hybrid" TN-ECB mode.
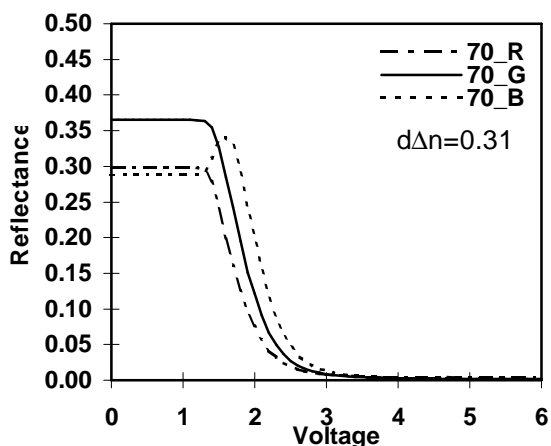

Fig.14 Reflectance vs. voltage relation of different parameters combinations(70°, 30°, 0.31)
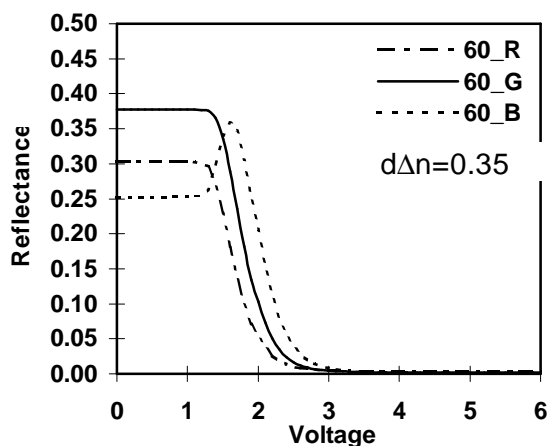
Fig.15 Reflectance vs. voltage relation of different parameters combinations(60°, 30°, 0.33)

Comparing the RVCs in Fig. 14 and 15, we find that the color dispersion of the new TN-ECB is much better than that of the SCTN.As a comparison, we list the contrast ratios of the MTN, SCTN and TN-ECB cells under different operating voltages in Table 1. One can select different parameter combinations to satisfy various needs of either low operating voltage or high contrasts. When $d\Delta n = 0.31\mu m$, for $\Delta n = 0.065$, the cell gap will be $5\mu m$, which is easily manufacturable. The dark operating voltage will be 4 V for a 74 contrast ratio.

RSTN MODE

By varying α, ϕ and $d\Delta n$ near the second TN-ECB minimum, it is possible to obtain a NW reflective mode with 100% light efficiency and low dispersion. In searching the parameter space, we concentrate on ϕ near 200-240° since this corresponds nearly to the common STN mode. The same optimization procedure as the RTN was used in optimizing the RSTN. Fig. 16 shows the calculated and experimental RVC for such an optimized RSTN. The experimental cell was fabricated in the usual manner with a 4-bottle LC system in order to adjust the $d\Delta n$ value. It can be seen that the RVC of the RSTN is rather sharp. A steepness coefficient of 1.2 can be obtained implying a

multiplexing capability of 30 lines. The threshold voltage is also reasonable. This RSTN therefore should be useful for pagers and PDA applications.

Figure 17 shows the dispersion curve for this RSTN. The dotted line is the experimental result while the solid line is the theoretical simulation. It can be seen that the agreement between them is rather good. More importantly, it can be noted that the RSTN is much more wavelength independent than a comparable STN display without film compensation. Typically the yellow mode of a STN has a 50% variation in reflectance in the visible. The RSTN on the other hand has only a 20% variation. Hence the RSTN can be used to make a good B/W display.
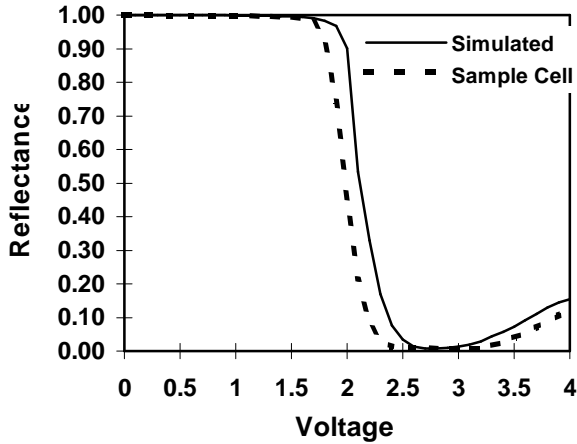

Fig.16 Comparison of experimental and theoretical RVC for the RSTN display.
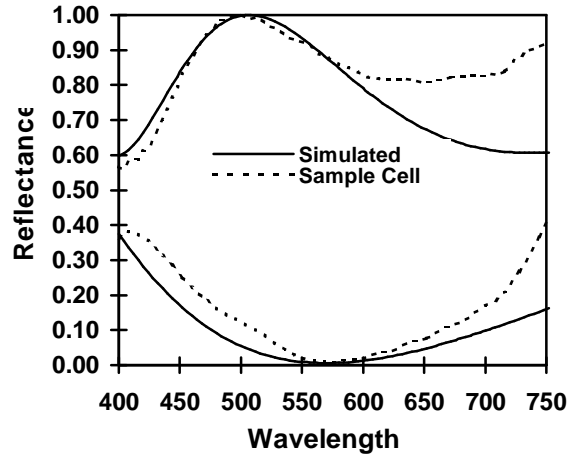

Fig.17 Comparison of experimental and theoretical reflectance spectra for the RSTN display.
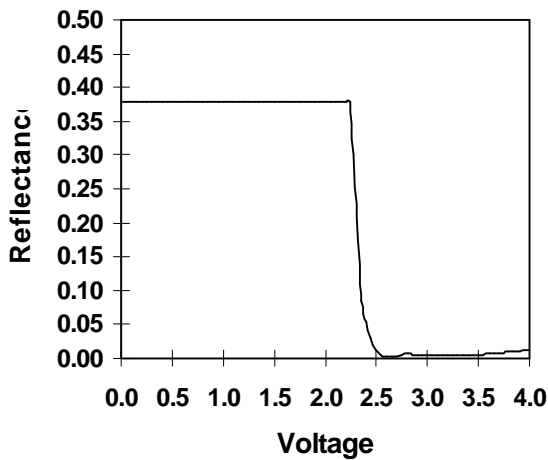

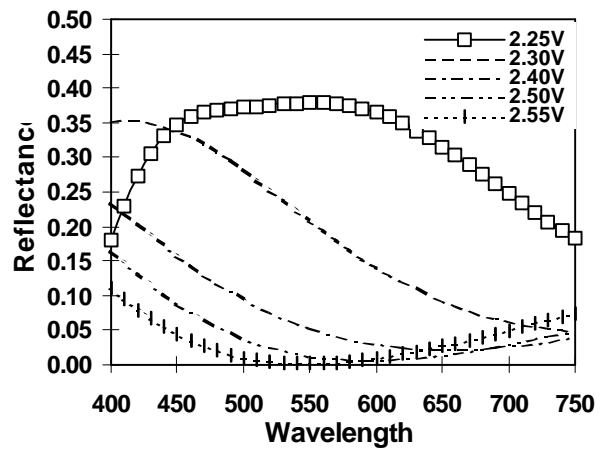Fig.18 The reflectance vs voltage curve using the conditions of point A in Fig.2

Fig.19 The complete RWCs for the voltage of 2.25 V, 2.30 V, 2.40 V, 2.50 V and 2.55 V using the conditions of point A in Fig.2

For higher mux numbers, the 200° cell does not provide a steep enough RVC. Fig.18 shows the case of a 240° twist cell with $d\Delta n = 0.85\mu m$ and $\alpha = 6^o$. It can be seen that a threshold voltage of 2.25V is obtained, followed by a sharp drop in reflectance. The steepness of this RVC is good enough for multiplex applications similar to transmissive STN. The V_{ns} is about 2.25 V and $V_s = 2.55$ V. Thus $V_s/V_{ns} \leq 1.13$, implying that a 100 lines multiplexing panel can be obtained. Another important observation about Fig. 18 is that R reaches to nearly 0% over a wide voltage range. Green light at 550 nm was assumed in this calculation. The complete reflectance spectra are shown in Fig. 19 for of 2.25 V, 2.30 V, 2.40 V, 2.50 V and 2.55 V respectively. It shows much lower dispersion as compared to conventional STN displays.

The significance of the results presented in Fig. 16-19 is that (1) A good contrast can be obtained with this new RSTN display. (2) The dispersion of the reflectance is excellent. It is better than transmissive STN LCD without film compensation. (3) High multiplexing of 100 lines can be obtained. We believe that after further optimization, higher multiplexing can be possible. This RSTN can replace conventional STN in many applications.

CONCLUSIONS

In this paper, we showed that by introducing the recently developed parameter space diagrams [14], many reflective twisted nematic modes that have excellent optical properties could be found. These new modes are related to the literature RLCD modes through a systematic variation of the LCD parameters. For the low twist case, it is called the RTN mode. This RTN has a mild reflectance-voltage behavior and is suitable for active matrix LCD. It is also ideally suitable for reflective projection displays.

The higher twist angle RSTN modes have twist angles near 200° and 240°. They are highly multiplexable and are suitable for passive matrix direct view LCD. Unlike the MTN mode, they do not require any quarterwave retardation plates for NW operation. Hence single polarizer sheet can be used in making a reflective display without backlighting. This display mode is suitable for PDA and pager applications.

We also showed an optimization of the MTN mode in this paper. The optimized MTN cell have high light throughput efficiency. In order to lower the operating voltage of the dark state and increase the cell gap, we also presented a modified SCTN mode which is just another TN-ECB mode. This new TN-ECB has large cell gap, low color dispersion and low operating voltage. It is quite suitable for crystal silicon CMOS driven active matrix LCD where the second polarizer cannot be applied.

ACKNOWLEDGMENTS

REFERENCES

1. J. Grinberg A. Jacobson, W. Bleha, L. Miller, L. Fraas, D. Boswell and G. Myer, "A real-time non-coherent to coherent light image converter, the hybrid field effect liquid crystal light valve, " Optical Engineering, 14(3), 217-225 (1975).
2. A. R. Kmetz, "A single-polarizer twisted nematic display, " Proceeding of SID, 21(2), 63-65 (1980).
3. T. Sonehara and O. Okumura, "A new twisted nematic ECB (TN-ECB) mode for the a reflective light valve, " Japan Display '89, Proc. of the 9th International Display Research Conference, 192-195 (1989).
4. T. Sonehara, "Photo-addressed liquid crystal SLM with twisted nematic ECB (TN-ECB) mode, " Jap. J. Appl. Phys., 29(7), L1231-L1234 (1990).

5. V. Konovalov, A. Muravksi, S. Yakovenko, A. Smirnov, A. Usenok, " A single-polarizer color reflective AMLCD with improved contrast, " SID 94 digest, 615-615 (1994).

6. K. Lu, B. E. A. Saleh, " Optimal twist and polarization angles for the reflective liquid crystal light modulator, " Journal of Modern Optic, 38(12), 2401-2410 (1991)

7. K. Lu, B. E. A. Saleh, "A single polarizer reflective LCD with wide-viewing-angle range for gray scales, " SID '96, Digest of Applications Papers, 63-66 (1996).

8. S. T. Wu and C. S. Wu, "High-brightness projection displays using mixed-mode twisted nematic liquid crystal cells, " SID '96, Digest of Technical Papers, 763-766 (1996).

9. S. T. Wu and C. S. Wu, "Mixed-mode twisted nematic liquid crystal cells for reflective displays, " Appl. Phys. Lett., 68(11), 1455-1457 (1996).

10. K. H. Yang, "A self-compensated twisted nematic mode for reflective light valve, ", Euro Display, 449-451 (1996).

11. S. T. Tang, M. Wong and H. S. Kwok, "Reflective twisted nematic liquid crystal displays," J. Appl. Phys. 81(9), 5924-5929 (1997).

12. I. Fukuda, M. Kitamura, Y. Kotani, "Electro-optical properties of a reflective STN-LCD with one polarizer and one retardation film, " Asia Display'95, Japan, 881-884 (1995).

13. I. Fukuda, E. Sakai, Y. Kotani, M. Kitamura, T. Uchida, "A new achromatic reflective STN-LCD with one polarizer and one retardation film, " Journal of the SID, 3(2), 83-87 (1995).

14. H. S. Kwok, "Parameter space representation of liquid crystal display operating modes, " J. Appl. Phys. , 80(7), 3687-3693 (1996).

15. G. H. Gooch and H. A. Tarry, "The optical properties of twisted nematic liquid crystal strustures with twist angles $\leq 90^\circ$" J.Phys. D**8,** 1575-1585 (1975).

16. H. L. Ong, "Origin and characteristics of the optical properties of general twisted nematic liquid-crystal displays, "· J. Appl. Phys., 64(7), 614-28. (1988)

17. T. Uchida, M. Suzuki, " A bright reflective LCD using optically compensated bend cell with gray-scale capability and fast response time, " SID '96, Digest of Technical Papers, 618-621 (1996).

18. H. Wóhler, "Numerical methods for parameter optimization of liquid crystal display," SID 91 Digest, 582-585 (1991).

19. D. W. Berreman, "Optics in stratified and anisotropic media: 4×4 matrix formulation," J. Opt. Soc. Am., 62(4), 502-510 (1972).

20. D. W. Berreman, "Optics in smoothly varying anisotropic planar structure: application to liquid crystal twist cells," J. Opt. Soc. Am., 63(11), 1374-1380 (1973).

21. H. Wóhler, G. Hass, M. Fritsch, and D. A. Mlynski, "Fast 4×4 matrix method for inhomogeneous uniaxial media," J. Opt. Soc. Am. A, 5(9), 1551-1557 (1988)

22. A. Lien, "Extended Jones matrix representation for the twisted nematic liquid-crystal display at oblique incidence," Appl. Phys. Lett., 57(26), 2767-2769 (1990).

23. K. H. Yang, "Elimination of the Fabry-Perot effect in the 4×4 matrix method for inhomogeneous uniaxial media," J. Appl. Phys., 66(4), 1550-1554 (1990).

24. K. H. Lu and B.E.A.Saleh, "Reducing Berreman's 4×4 formulation of liquid crystal display optics to 2×2 Jones vector equations, " Opt. Lett., 17(22), 1557-1559 (1993).

25. P. Yeh, "Extended Jones matrix method," J.Opt.Soc.Am. A, 72(4), 507-513 (1983)

26. C. Gu, P. Yeh, "Extended Jones matrix method. II," J.Opt.Soc.Am. A, 10(5). , 966-973 (1993).

27. P. Yeh, *Optical Waves in Layered Media* (Wiley, New York, 1988), 201-253.

28. F. H. Yu, J. Chen, S. T. Tang and H. S. Kwok, "New extended Jones matrix method for twisted nematic liquid crystal display at oblique incidence " SPIE, 2894, 17-28 (1996).

29. J. Chen, F. H. Yu, S. T. Tang and H. S. Kwok, "Chromatic parameter space representation of LCD operating modes," IDRC'97, Canada.

30. H C Huang, C T Nguyen and H S Kwok, "Planarization of liquid-crystal-on silicon projection display with multilevel metallization and chemical-mechanical polishing," SID 96 Symposium Digest, p. 685-688(1996).